J Mater Sci (2009) 44:2725–2735
DOI 10.1007/s10853-009-3330-1

Nanocrystalline alumina dispersed in nanocrystalline nickel: enhanced mechanical properties

A. Jung · H. Natter · R. Hempelmann · E. Lach

Received: 1 August 2008 / Accepted: 9 February 2009 / Published online: 3 April 2009

Abstract Nickel–alumina nano-composites have been electrochemically deposited by pulse plating from a suspension of nano-Al_2O_3 in a Watts-type electrolyte. The influence of duty cycle and amount of suspended Al_2O_3 on the content of Al_2O_3 in the deposit was studied. With an optimized set of plating parameters, the influences of additives on wear resistance, hardness and the deformation behaviour (quasistatic and dynamic compression tests) of these nickel–alumina nano-composites in comparison to pure nano-nickel were investigated. The addition of Al_2O_3 tripled the yield stress and improved the hardness up to twice the value of pure nickel. Due to its high hardness and stiffness, the nickel–alumina composites deposited with the additive naphthalene-1,3,6-trisulfonic acid trisodium salt in the electrolyte are appropriate to wear resistant coating. Nickel–alumina nano-composites deposited without any additives are hard and at the same time ductile and so considered as ideal structural materials.

Introduction

In our highly engineered world, there are more and more requirements on the properties of construction materials. The material should be light but also robust; it should offer the combination of several mechanical properties like hardness, wear resistance, in some cases self-lubrication, heat resistance and, simultaneously, it should have good anticorrosion properties. These requirements can no longer be fulfilled by a monolithic material, and hence the interest in composites. Metal matrix composites (MMCs) consist of inert second phase particles, usually ceramic particles, dispersed in a metallic matrix. The inert particles can be hard oxides such as Al_2O_3 [1–3], ZrO_2 [4–6], TiO_2 [7–9] or carbides like SiC [10–12], WC [13–15], TiC [16, 17] or even diamond particles [18–20]. For self-lubrication applications, the second phase consists of PTFE [21–23], carbon nanotubes [24–26], graphite or MoS_2 [27–29]. The advantage of particle-reinforced MMCs compared to fibre-reinforced composites is the isotropic microstructure which offers an isotropic behaviour in material testing.

An application for MMCs is the coating of base materials. Particle-reinforced composite coatings based on nickel and alumina are being applied in different fields of technology with high demands on friction and corrosion resistance. Examples are the paddles of gas turbines, the mixing blades for abrasive mixtures and other surfaces with appearance of wear [2, 30].

There are several preparative routes to MMCs: powder-metallurgical methods [31–34], squeeze casting [35, 36], physical and chemical vapour deposition (PVD and CVD) [31, 37], High Velocity Oxygen fuel thermal (HVOF) spraying [31, 38, 39], electrophoretic deposition [31, 40–42], electrolytic deposition [2, 3, 30, 43].

In this article, electrochemical deposition by pulse plating, which is a very versatile method, is used [44, 45]: apart from the type, shape and amount of the particles dispersed in the electrolyte, the properties of the deposited composite can be tuned by the variation of the plating parameters such as current density, duty cycle, pulse repetition rate and so on. The duty cycle is the ratio of pulse duration (on-time) and sum of on- and off-time.

A. Jung · H. Natter (✉) · R. Hempelmann
Physical Chemistry, Saarland University,
66123 Saarbrücken, Germany
e-mail: h.natter@mx.uni-saarland.de

E. Lach
ISL, French-German Research Institute of Saint-Louis,
68301 Saint-Louis, France

The exact mechanism for co-deposition of inert particles dispersed in an electrolyte in a metallic matrix by electro-deposition is far from being well understood. There are four mechanisms which are discussed, namely electrophoresis [46], convective diffusion [47], mechanical entrapment [48] and adsorption [49] of the particles on the cathode.

Since the year 1970, several theoretical models have been developed to describe the co-electro-deposition of inert particles and metal ions. Subsequently, two common models are briefly outlined, namely the model of Guglielmi [50] and the model of Celis et al. [51].

The mechanism proposed by Guglielmi [50] is based on two steps (Fig. 1). The first step is a loose physical adsorption of the particles on the cathode with a high degree of coverage and without discharge of the electro-active ions adsorbed on the particles. The fractional coverage follows a Langmuir adsorption isotherm. The second step is the strong electrochemical adsorption of the particles by the applied electrochemical field accompanied by the discharge of the electro-active ions. Both steps take place at the same time all over the surface of the cathode. If a particle is strongly adsorbed on the cathode, it will be embedded in the growing metal layer by the electro-deposition also of free solvated electro-active ions from the plating bath. The deficiencies of the model are the neglect of hydrodynamics, particle size and ageing effects. Strictly speaking, a Langmuir isotherm, valid for molecular chemisorption, is hardly applicable to large particles. Hence, other models have been developed.

One of the common new models is the model of Celis et al. [51] which accounts for hydrodynamics and is based on five steps:

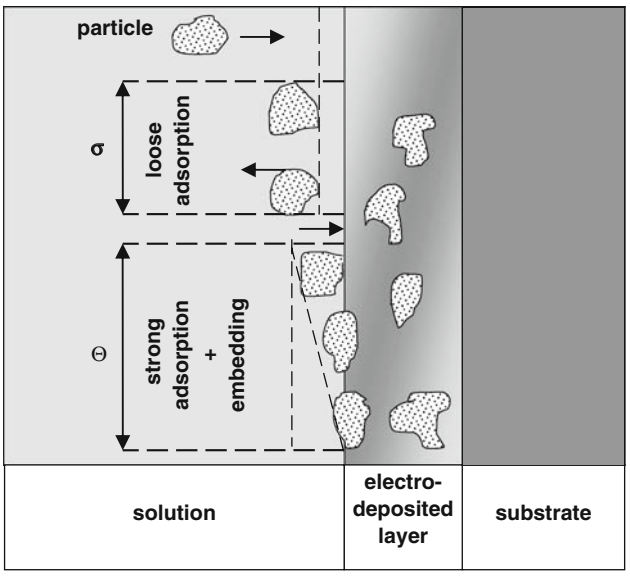

Fig. 1 Scheme of the two-step deposition process by Guglielmi (σ is the coverage by loose adsorption and Θ is the coverage by strong electrochemical adsorption)

1. Formation of an ionic cloud around the particles,
2. Transport of the particles by convection to the hydrodynamic boundary layer,
3. Transport of the particles by diffusion to the cathode,
4. Free ions and electro-active ions adsorbed on the particles are adsorbed at the cathode, and
5. Electrochemical reduction of the absorbed ions at the cathode with the embedding of the particles into the growing metallic matrix.

In this article, nickel/alumina (Ni/Al_2O_3) MMCs are electrochemically prepared with optimization of the particle content. The superior mechanical properties of the resulting metal matrix nanocomposites are demonstrated.

Mechanical properties

According to Hornbogen [52], the ductile deformation of a particle-strengthened composite can be approximated by a series of micromechanical elements. In this study, the constituents are a metallic matrix, and hard particles dispersed in this matrix. If there is a mechanical load on such a composite, the stresses σ on the hard particles and on the matrix material are equal, but the strains ε are different. The strain of the composite is a function of the volume fractions f and the partial strains σ of the metallic matrix (α) and the hard material (β), respectively:

$$\varepsilon = \varepsilon_\alpha \cdot f_\alpha + \varepsilon_\beta \cdot f_\beta. \quad (1)$$

If there is no ductile deformation of the hard material ($\varepsilon_\beta = 0$), the plastic deformation of the composite is only due to the matrix material ($\varepsilon = \varepsilon_\alpha f_\alpha$).

Particle strengthening of metals

An increase in the hardness of a material is always associated with an increase in its resistance against ductile deformation and thus against the generation and sliding of dislocations. For the nano-MMCs produced in this study, there are two possible hardening and strengthening mechanisms: the hardening by grain refinement [53] of the matrix and the dispersion hardening by particles [54], respectively. The particles act as obstacles to dislocation movements and cause the hardening of the material. The hardening by grain refinement is based on the increasing number of grain boundaries and triple junctions due to the decreasing grain size. In this case, the grain boundaries and triple junctions act as obstacles to the dislocation movement.

There are several mechanisms which describe the interactions of the dislocations with the dispersed particles in the metal matrix. Common mechanisms are the particle bypassing by Orowan looping or particle shearing.

The hardening by particles due to particle shearing takes place only for coherent particles with a similar lattice structure as that of the host metal. If a dislocation strikes a particle, the dislocation enters into the particle, passes through and shears it on a slipping plane. This causes new additional surface area which requires interfacial energy and is responsible for the strengthening of the material.

In the case of incoherent particles, the hardening is explained by the Orowan looping mechanism [55] which in its classical form is analogue to dislocation multiplication by a Frank–Read source. Mobile dislocations attach on the particles and bulge at the particles due to the Peach–Köhler force which causes elongation of the dislocation. The bowing of the dislocation increases, as the force acting on the dislocation increases. There is a balance between the Peach–Köhler force and the line tension T_L of the dislocation which tends to shorten the dislocation. The critical radius of curvature, where the bowing of the dislocation is maximized, is half of the particle interspacing, L. The necessary tension for this bowing, the so-called Orowan tension τ_{crit}, is given by the Orowan equation

$$\tau_{crit} = \frac{2T_L}{b \cdot L} \tag{2}$$

with the Burgers vector b. At the Orowan tension, parts of the dislocation with different signs are opposite to each other and attract each other. This creates a loop around the particle. The loop tears, and a dislocation ring remains around the particle while the main part of mobile dislocation moves forward. After the passing by over a dislocation and the creation of a dislocation ring around the particle (Orowan-loop), the particle remains unchanged, i.e. undeformed. This process requires energy and is therefore responsible for the hardening effect by Orowan. According to the Orowan equation, the magnitude of hardening is inversely proportional to the interparticle spacing. Therefore, for a given volume fraction, smaller particles are more efficient (larger τ_{crit}) because their number density is larger and thus their interparticular distance is smaller.

The mechanisms outlined above are not the only interaction mechanisms of dislocations with the dispersed particles which cause a hardening effect. The particles can also be circumvented by climbing or cross-slipping of the dislocations. Possible is even a combination of the above effects [56].

Wear behaviour of MMCs

There are three kinds of wear, namely adhesive wear, abrasion and surface fatigue wear. This article deals only with the abrasion. Abrasion is caused by the penetration of hard asperities of a material into another softer material. If there is movement between the two bodies, the softer one will be grooved by the harder one. Particularly for abrasive wear, the hardness of a specimen is directly proportional to its wear resistance [57]. The wear resistance of metals can be improved by the embedding of hard particles like oxides, carbides or diamond particles. The hard particles act as obstacles for the penetration of hard asperities of other materials and thus decrease the wear.

A standard method to determine the abrasive wear is the Taber Abraser method. Measure for the quantification of abrasive wear is the weight loss as expressed in the Taber wear index (TWI). The TWI is determined as the weight loss per 1000 cycles. The TWI according to the volume loss method is the weight loss per density of the specimen per 1000 cycles. To compare samples which have different densities, the TWI according to the volume loss method should be used.

Strain-rate sensitivity

A lot of materials are strain-rate sensitive depending on their microstructure. The generation of dislocation or obstacles with short-range effect are responsible for the strain-rate sensitivity. The nanocrystalline nickel studied in this investigation belongs to the strain-rate sensitive materials resulting in increasing strength at increasing strain rate. This is due to the rapid increase in dislocation density at the onset of dynamic plastic deformation. The strain-rate sensitivity m is defined as

$$m = \frac{\Delta(\ln \sigma)}{\Delta(\ln \dot{\varepsilon})}. \tag{3}$$

It is determined by the difference between the stresses σ in quasistatic and dynamic tests and the difference in strain rate $\dot{\varepsilon}$ of the quasistatic and dynamic tests for a given strain. The dependence of the strain-rate sensitivity on the strain gives information about the governing hardening mechanism [58]. In the case of pure dislocation–dislocation interactions, the strain-rate sensitivity is independent of the strain magnitude. A decreasing value of the strain-rate sensitivity with increasing strain indicates lattice friction or pinning of dislocations, e.g. at particles dispersed in a metallic matrix [58].

Materials and methods

Plating conditions

Nickel and Ni/Al_2O_3 composite coatings were electrochemically deposited from a Watts type electrolyte by pulsed electro-deposition (PED). The composites were deposited from electrolytes with different amounts of

Table 1 Composition of the modified Watts electrolyte

Composition of the Watts electrolyte	(g/L)
$NiSO_4 \times 6H_2O$	281
$NiCl_2 \times 6H_2O$	60
H_3BO_3	30
Sodium dodecyl sulphate (SDS)	0.2

alumina powder (Baikalox—Ultra-High Purity Alumina by Baikowski, Annecy, with a medium diameter of 45 nm according to the manufacturer). The composition of the modified Watts electrolyte is given in Table 1.

The depositions were carried out at a bath temperature of 50 °C and a pH of 4.1. For the preparation of the dispersion, first, the alumina powder was dispersed in the Watts electrolyte using a high velocity disperser (Ultra Turrax from IKA, Freiburg) for 30 min. Then, sodium dodecyl sulphate (SDS) and other organic additives were added to the dispersion, and it was ultrasonicated for 30 min. During the deposition, each plating bath was agitated by a magnetic stirrer with a rotation speed of 360 rpm. The depositions were carried out in 400 mL electrolysis cells. A rectangular iron plate of an area of 36 cm^2 was used as cathode. Before plating, the iron was electroless coated with a thin copper film in order to facilitate the removal of the deposit from the cathode after the deposition. The sacrificial anode (counter electrode) consists of a titanium basket filled with nickel pellets (A.M.P.E.R.E. GmbH).

The depositions were carried out with various duty cycles and various amounts of α-alumina in the plating bath with a pulse current density of 20 mA/cm^2 and a pulse repetition rate of 20 Hz. With an optimized set of parameters (30% duty cycle, 120 g/L Al_2O_3 in the plating bath), the effect of organic additives on the deposit's particle content, surface morphology, texture, hardness, wear resistance and the material behaviour under compressive loading was studied. Equimolar amounts of well-known grain refiner were used as additives in order to provide an additional strengthening of the deposits. The effect of the sodium salt of saccharine (3.54 g/L) and the trisodium salt of naphthalene-1,3,6-trisulfonic acid (7.5 g/L) which do also reduce the internal stresses of the deposits was studied.

Characterization

In order to determine the amount of incorporated alumina in the composites, we have measured the density of the composite samples using Helium pycnometry which is a non-destructive method and does not require special sample geometries, an advantage in relation to gravimetric methods. Because of the large difference in density between the nickel matrix and the incorporated alumina particles, the volume fraction ϕ of particles in the composites could be evaluated according to the following equation.

$$\phi = \frac{\rho_S - \rho_{matrix}}{\rho_{particle} - \rho_{matrix}} \quad (4)$$

where ρ_S is the measured density of the specimen and ρ_{matrix} and $\rho_{particle}$ are the literature values of the densities of the matrix (Ni) and of the dispersed particles (α-Al_2O_3), respectively.

The nanocrystalline matrix, the nanocrystalline particles and the texture of the composites have been identified by X-ray diffractometry (XRD; Siemens D500).

The surface morphology and the successful incorporation of the alumina particles have been visualized by scanning electron microscopy (SEM) equipped with energy dispersive X-ray spectroscopy (Jeol JSM 7000 F).

Hardness and wear resistance

The hardness was measured using a Vickers microindenter (Leica VMHT MOT) under a load of 980.7 mN on coatings with thicknesses of about 300 μm.

The wear resistance was tested on a Taber Abraser model 5131. Taber S-16 plates were plated with pure nickel and nickel–alumina composite coatings from the Watts-type electrolyte. The wheels used in the test were CS-10 wheels under a load of 1000 g on each wheel. The tests were conducted in two steps. For the first 1000 cycles, the weight loss in mg was determined per 200 cycles. From 1000 to 10,000 cycles, the weight loss was determined per 500 cycles. Because of the abrasion of the wheels, they were reground after every 1000 cycles. The Taber wear index (TWI) according to the volume loss method was evaluated from the weight loss and the density of the constituent material.

Quasistatic and high dynamic compression tests

The quasistatic compression tests were carried out at strain rates about 2×10^{-3} s^{-1} using a universal testing machine (INSTRON 4204, Instron GmbH).

Compression tests at high dynamic loading were conducted on a classical split-Hopkinson-pressure-bar (SHPB) reaching strain rates up to 5×10^3 s^{-1}. The theory of the Hopkinson bar technique is based on the one-dimensional propagation of elastic waves. Additional assumptions are: uniaxial stress conditions in the specimen, friction between bars and specimen, and the inertia effects are negligible. Figure 2 shows the scheme: The SHPB consists of a gas gun and four cylindrical elastic bars, the projectile or the so-called striker bar, the incident bar, the transmission bar and the damping bar. The short cylindrical sample is placed between the incident and the transmission bar. The striker

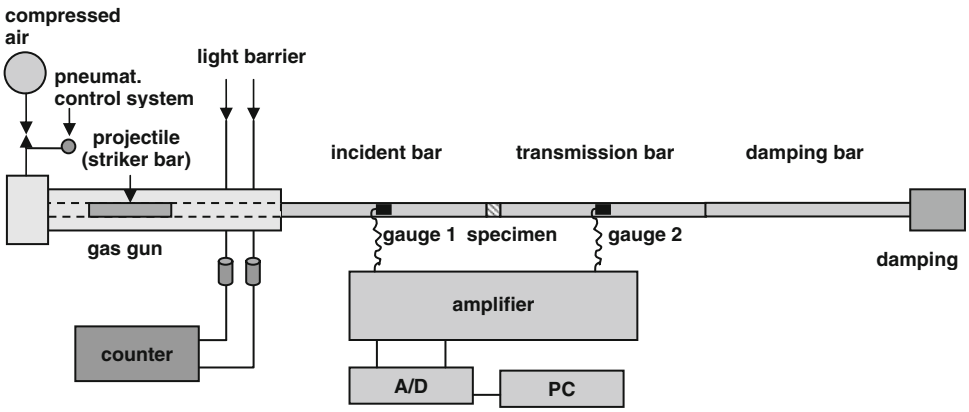

Fig. 2 Design of a split-Hopkinson-pressure-bar apparatus

bar is accelerated by the gas gun. When the striker bar impacts the front section of the incident bar, an impact momentum is generated in the incident bar and propagates as an elastic, longitudinal compression wave through the bar. At the incident bar/sample interface, there is an impedance mismatch with the incoming wave being partly transmitted into the transmission bar and partly reflected into the incident bar. The three waves (incoming, reflected and transmitted) are measured as longitudinal strains versus time using strain gauges. From the signals of the strain gauges, a stress–strain diagram can be plotted.

The dynamic compression tests of this study had been performed on the SHPB of ISL at strain rates of about 3500 s^{-1}. It gives information on the dynamic materials' responses of pure nano-nickel and nickel/alumina composites under compressive loading. The specifications of the SHPB apparatus are listed in Table 2.

Results and discussion

Optimisation of the particle content

Figure 3 shows the dependence of the particle content on the duty cycle. A decrease in duty cycle leads to an increase of the alumina content in the composite. This increase of particle content with decreasing duty cycles is probably due to the shorter pulse-on-time and the longer pulse-off-time. During the longer pulse-off-time, more Al_2O_3 particles which carry adsorbed Ni ions, reach the cathode by convection and diffusion. In the subsequent pulse-on-time, the ions absorbed on the particles will be discharged and the particles will be embedded into the growing metal layer. Because of the short pulse-on-time the deposition of the free Ni ions during a pulse is reduced.

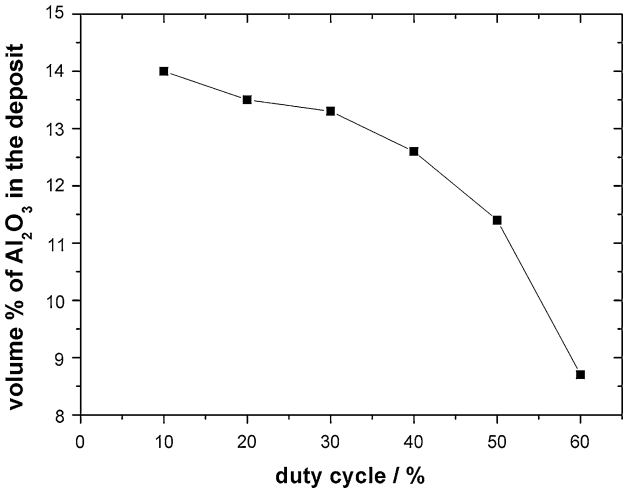

Fig. 3 Effect of pulse duty cycle on the alumina content of the composite

The dependence of the alumina content in the deposit on the particle content in the plating bath is shown in Fig. 4. The higher the particle amount in the plating bath, the higher the alumina content in the deposits, up to a maximum saturation value. According to Guglielmi's suggestion, these data have been fitted with a function analogous to the Langmuir isotherm. The saturation alumina content was determined as 18.0 vol.% and the constant of the assumed Langmuir isotherm K = 0.03 L/g was obtained.

Table 2 Technical data of the bars and the striker bar

Technical data of the bars and the striker		
Incident- and transmission-bar	Material	Tool Steel Böhler S390
	Length L (mm)	1400
	Diameter ∅ (mm)	12
	Wave propagation rate (m/s)	5391
Striker bar	Material	Maraging steel
	Length L (mm)	500
	Diameter ∅ (mm)	12
	Mass m (g)	400

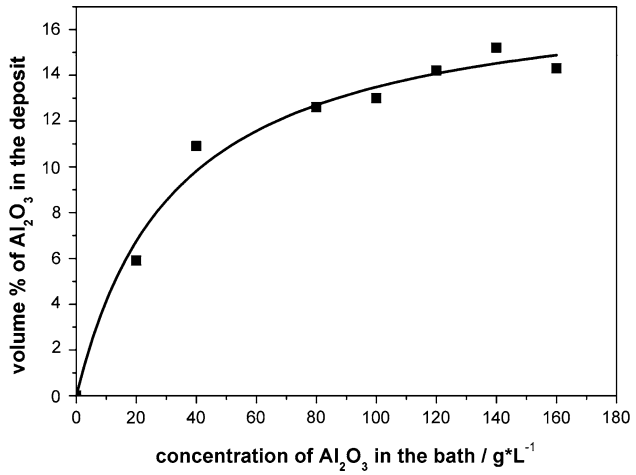

Fig. 4 Effect of concentration of alumina in the bath on the alumina content of the composite

Lower duty cycles and higher particle loadings of the plating bath bring about longer plating times. So a compromise must be made between the alumina content of the composite and the plating time. For further depositions, the following parameters were used: 30% duty cycle and a particle concentration of 120 g/L in the electrolyte.

XRD analyses of the coatings

Table 3 shows the relative intensities of the Bragg reflections in the XRD patterns of the Ni/Al_2O_3 composites prepared without additives depending on the duty cycle and in the particle concentration of the plating bath. The main growth orientation in these composites is (111). The higher the duty cycle, the lower is the (220) reflection intensity. The same holds true for an increase in the alumina concentration of the plating bath. The change in the intensities of the other reflections is much less pronounced both for a change in the duty cycle and in the particle concentration. Evidently, by changing the particle loading in the plating bath or the duty cycle, one can modify the metallic matrix.

The XRD patterns of pure n-nickel deposited with the sodium salt of saccharine and of the Ni/Al_2O_3 composites deposited without additives and with the sodium salt of saccharine and the naphthalene-1,3,6-trisulfonic acid trisodium salt, respectively, are displayed in Fig. 5. All the deposits with additives form strong (200) textures. In the composite deposited with saccharine, all the grains have the same growth direction. The composite, deposited without any additives, shows a strong (111) texture. Hence, the addition of additives to the plating bath has a strong influence on the main growth direction of the composite layers.

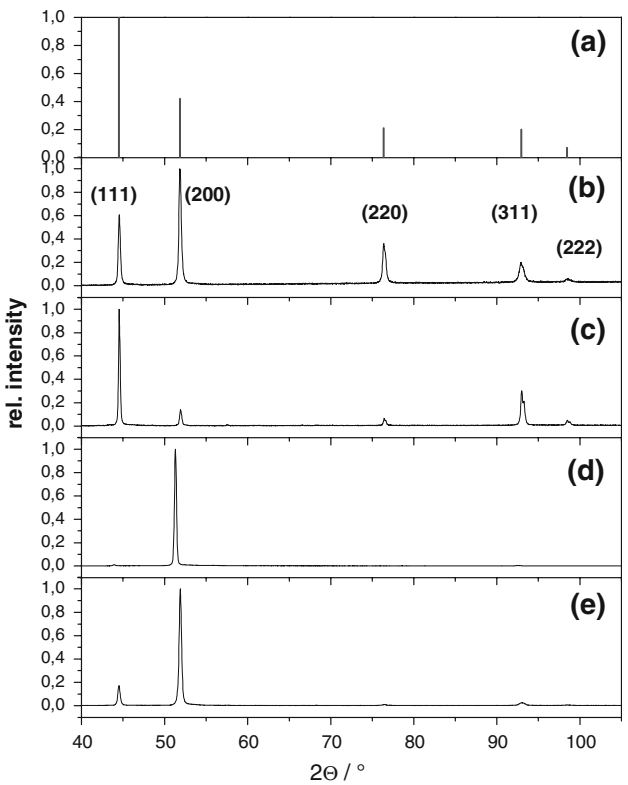

Fig. 5 XRD pattern of **a** 04-850 Ni, syn; **b** pure nickel + Na-saccharine; **c** Ni/Al_2O_3; **d** Ni/Al_2O_3 + Na-saccharine; **e** Ni/Al_2O_3 + Na-naphthalene-1,3,6-trisulfonic acid

The grain sizes of the different Ni/Al_2O_3 composite coatings are shown in Table 4. The grain sizes have been determined by the Scherrer method, which disregards microstrains, and for all the samples, about the same grain size results.

Table 3 Relative intensities of the main X-Ray Bragg reflections depending on a change in duty cycle or concentration of Al_2O_3 in the plating bath

	Duty cycle			04-850 Ni, syn	Concentration of Al_2O_3		
	10%	40%	60%		40 g/L	80 g/L	120 g/L
(111)	1.00	1.00	1.00	1.00	1.00	1.00	1.00
(200)	0.25	0.19	0.19	0.42	0.25	0.19	0.14
(220)	0.32	0.13	0.12	0.21	0.30	0.13	0.06
(311)	0.16	0.11	0.13	0.20	0.15	0.12	0.12

Table 4 Crystallite size and texture of the nickel matrix and amount of alumina in the deposits

	Additive	Crystallite size (nm)	Texture	Vol.% of Al_2O_3
Pure Ni	Na-saccharine	49	(200)	–
Ni/Al_2O_3 composites	–	56	(111)	14.8
	Na-saccharine	58	(200)	5.1
	Na-naphthalene-1,3,6-trisulfonic acid	49	(200)	15.5

Surface morphology and microstructure of the coatings

The surface morphology of the coatings as-deposited, visualized by scanning electron microscopy (SEM), is strongly effected by the different additives (Fig. 6). The composite coating deposited without any additive is made up of regular pyramidal grains. On the other hand, the composite deposited with the sodium salt of saccharine has grains in the form of pebbles and that deposited with the trisodium salt of naphthalene-1,3,6-trisulfonic acid shows no visible grain boundaries in SEM.

The cross-sections of the composites (Fig. 7) show a rather homogeneous distribution of small particle agglomerates for the composites without additives and with the trisodium salt of naphthalene-1,3,6-trisulfonic acid, respectively. The particle content of the layer deposited with the sodium salt of saccharine is much lower. The particle content determined by pycnometry is 14.8 vol.% for Ni/Al_2O_3, 5.1 vol.% for Ni/Al_2O_3 with Na-saccharine and 15.5 vol.% for Ni/Al_2O_3 with Na-naphthalene-1,3,6-trisulfonic acid. Obviously, the addition of Na-saccharine lowers the particle content to about one-third of that of the deposition without any additive. For the composite prepared with the addition of Na-naphthalene-1,3,6-trisulfonic acid, there is a slight increase in the amount of particles embedded into the nickel matrix.

The physical and structural properties of all the four samples are listed in Table 4.

Wear resistance of Ni and Ni–Al_2O_3 composite coatings

Figure 8 maps the wear versus stroke characteristics of the Ni/Al_2O_3 composites and a pure nickel sample. The pure nickel sample and the composite deposited with Na saccharine have almost the same material behaviour. The slope of the graph and so the average wear rate is more than twice that of Ni/Al_2O_3 and Ni/Al_2O_3 with Na-naphthalene-1,3,6-trisulfonic acid. The two samples, Ni/Al_2O_3 and the sample with Na-naphthalene-1,3,6-trisulfonic acid, show a similar material. The wear resistances of the latter two composites are more than twice the wear resistance of the pure n-nickel and the composite with Na-saccharine. The improved wear resistance is probably due to the higher

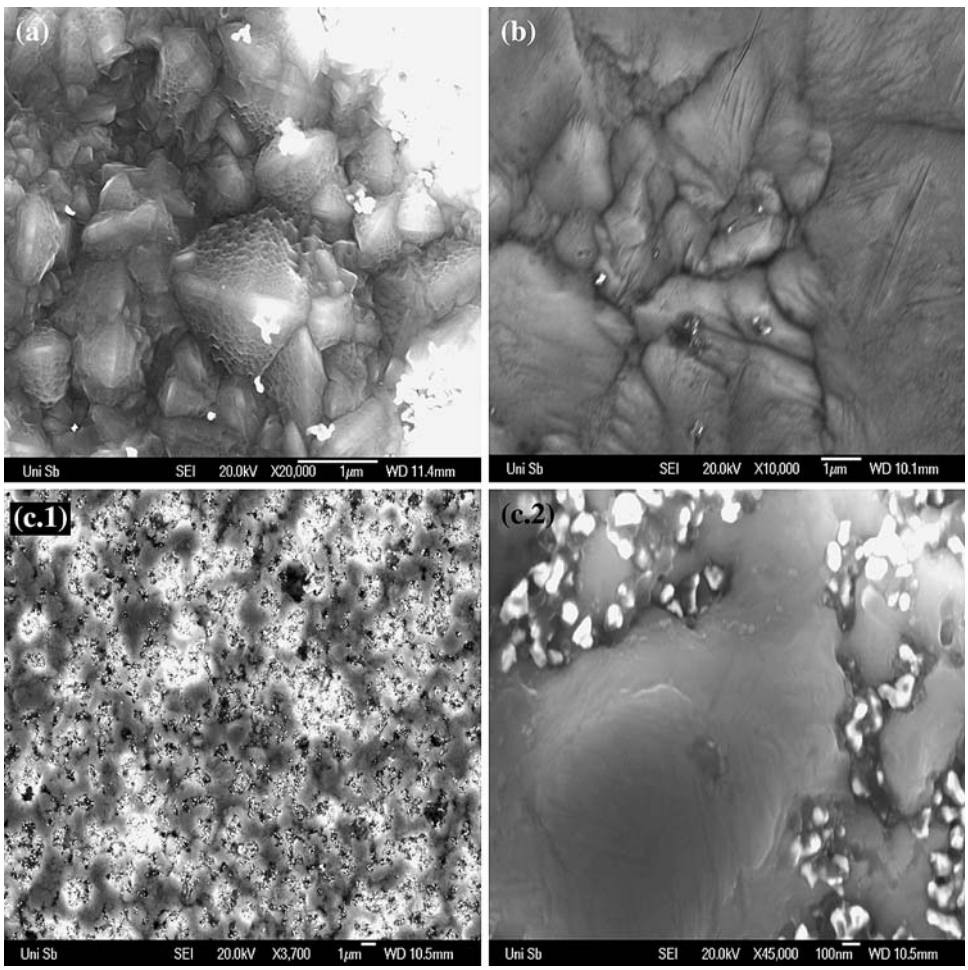

Fig. 6 SEM images of **a** Ni/Al_2O_3; **b** Ni/Al_2O_3 + Na-saccharine; **c** Ni/Al_2O_3 + Na-naphthalene-1,3,6-trisulfonic acid

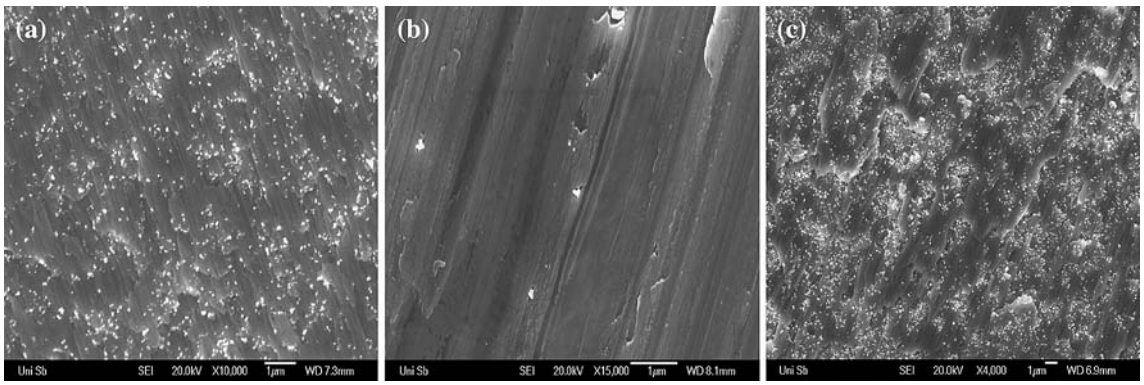

Fig. 7 SEM images of the cross-sections of **a** Ni/Al_2O_3; **b** Ni/Al_2O_3 + Na-saccharine; **c** Ni/Al_2O_3 + Na-naphthalene-1,3,6-trisulfonic acid

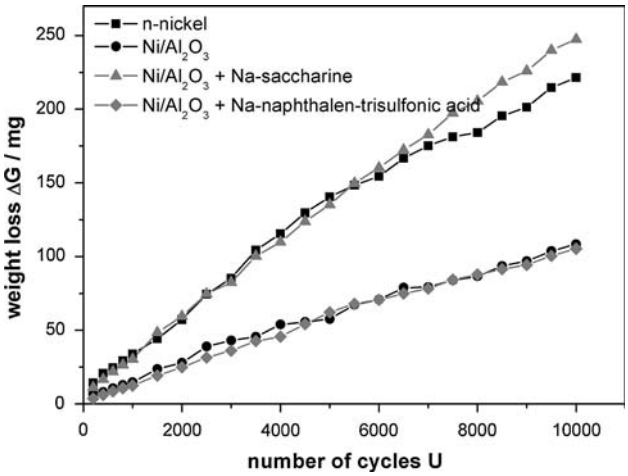

Fig. 8 Wear vs. stroke characteristics of pure nickel and Ni/Al_2O_3 composites

amount of particles embedded in the nickel matrix. The composite with Na-saccharine has the wear resistance similar to that of the pure n-nickel, but in the case of high duty cycles, it is worse than n-nickel. This led to the suggestion that a particle content of 5.1 vol.% of alumina is too low to improve the wear behaviour. The worse behaviour in the case of high duty cycles might be due to the strong texture of this sample, which exhibits essentially only one growth direction. According to Fisher [59], texture formation in a metal deteriorates its hardness

Table 5 summarizes several wear characteristics of the four samples.

Hardness of Ni- and Ni–Al_2O_3 composite coatings

Table 6 shows the measured values of the hardness of the four samples and of a second pure nickel sample with a larger grain size. The differences in hardness between the two pure nickel samples are probably due to the different grain sizes. According to Hall-Petch, a sample with a smaller grain size is harder because of the increase in grain boundaries and triple junctions which act as obstacles for the dislocation movement. The increase in hardness of the three composites is due to the particles that are embedded. The differences between the composites are due to the different particle contents of the composites. The lower the particle content, the lower the measured value of the hardness. Because of the particle content which is only 5.1 vol.%, the Ni/Al_2O_3 composite with Na-saccharine exhibits the lowest hardness of the composites but it turns out to be still harder than the pure nickel sample with almost the same grain size. The Ni/Al_2O_3 composite prepared with the addition of Na-naphthalene-1,3,6-trisulfonic acid has the largest particle content (15.5 Vol.%) among the composites, and it exhibits, consequently, the highest hardness.

Quasistatic and dynamic compression tests on Ni and Ni–Al_2O_3 composite samples

Figure 9 summarizes the quasistatic and dynamic compression tests performed on nickel and nickel composite specimens. In a SHPB-test, there is insufficient stress

Table 5 Wear characteristics ($\dot{\Delta}G_m$ is the average abrasion rate)

	Mass loss (mg)	Loss of thickness (μm)	$\dot{\Delta}G_m$ (mg/cycle)	TWI_V (after 10,000 cycles)
N-nickel + Na-saccharine	221.5	8.3	0.022	2.5
Ni/Al_2O_3	108.4	4.4	0.010	1.3
Ni/Al_2O_3 + Na-saccharine	247.5	9.6	0.025	2.9
Ni/Al_2O_3 + Na-naphthalene-1,3,6-trisulfonic acid	105.3	4.3	0.010	1.3

Table 6 Vickers hardness of the pure nickel and Ni/Al_2O_3 composites

	n-nickel	n-nickel + Na-saccharine	Ni/Al_2O_3	Ni/Al_2O_3 + Na-saccharine	Ni/Al_2O_3 + Na-naphthalene-1,3,6-trisulfonic acid
HV 0.1/15	200	244	406	285	429

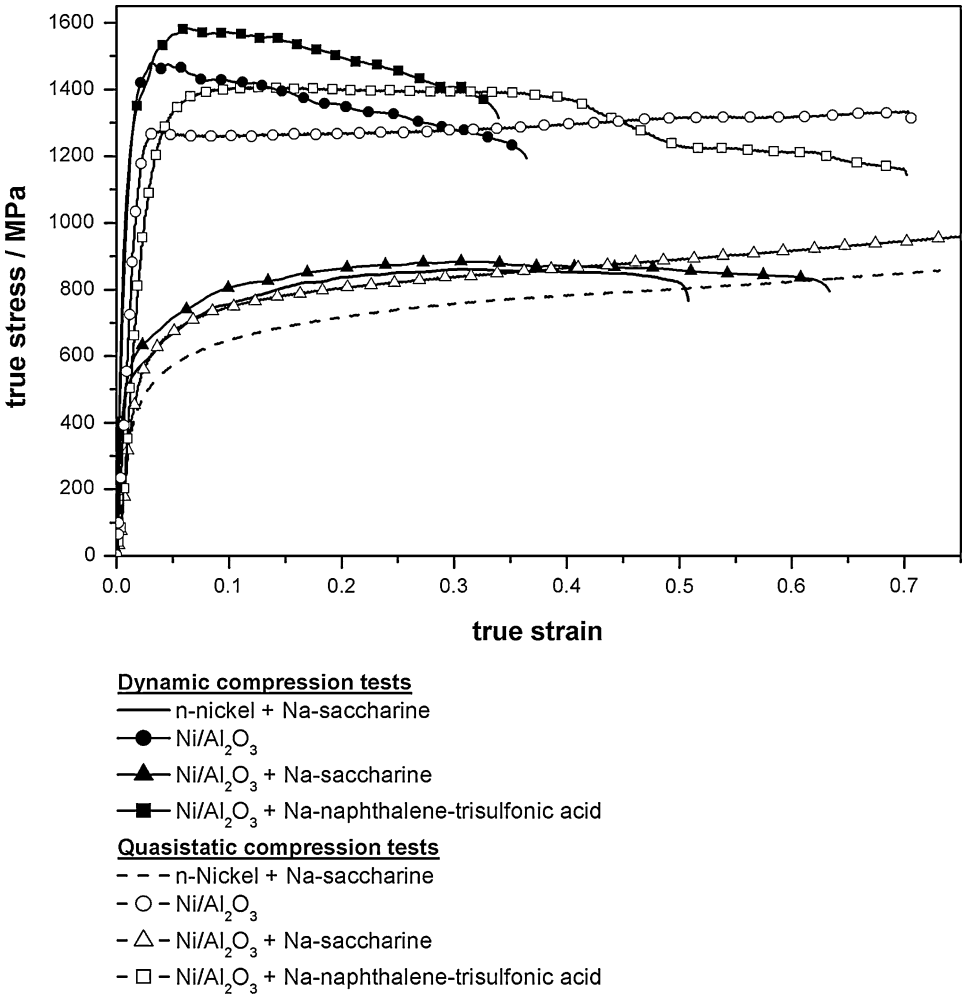

Fig. 9 Stress–strain characteristic of the quasistatic and dynamic compression tests

equilibrium at small strains; for this reason, in dynamic flow curves, flow stresses are evaluated from a plastic strain of 3% onwards [60]. Therefore, the offset flow stress under dynamic loading is defined at 3% of plastic deformation. The values for the 0.2% and 3% offset flow stresses of the compression flow curves measured in quasistatic mode, and the 3% offset flow stresses of the dynamic flow curves are listed in Table 7. The two composites with the high particle content (Ni/Al_2O_3 and Ni/Al_2O_3 with Na-naphthalene-1,3,6-trisulfonic acid) have 3% offset flow stresses of more than twice of that of the pure nickel and the composite deposited with Na-saccharine. In quasistatic compression test, there was only a fracture in Ni/Al_2O_3 with Na-naphthalene-1,3,6-trisulfonic acid. In dynamic compression tests, there was no fracture. While the composite with Na-saccharine exhibits better mechanical properties than those of the pure nickel in quasistatic compression tests, in dynamic tests there was almost no difference between the two samples in their mechanical behaviour.

Due to the enhanced rate of dislocation movement, there is an increase in the flow stress in the dynamic compression tests.

The decrease of the flow stress caused by the two composites with the higher particle content depends on the adiabatic heating and the increased internal friction due to the dynamic loading and the increased particles content, respectively.

Table 8 shows the strain-rate sensitivity of the samples for a strain of 10% and 20%. The negligible strain-rate sensitivity of the pure nickel and the composite deposited

Table 7 3% offset flow stresses of the pure nickel and Ni/Al_2O_3 composites

	Flow stress R_{P3} (MPa)	
	Quasistatic	Dynamic
n-nickel + Na-saccharine	599	634
Ni/Al_2O_3	1330	1527
Ni/Al_2O_3 + Na-saccharine	714	694
Ni/Al_2O_3 + Na-naphthalene-1,3, 6-trisulfonic acid	1463	1554

Table 8 Strain-rate sensitivity for 10% and 20% of strain

	$m_{10\%}$	$m_{20\%}$	Δm
n-nickel + Na-saccharine	0.0110	0.0108	0.0002
Ni/Al_2O_3	0.0089	0.0048	0.0041
Ni/Al_2O_3 + Na-saccharine	0.0052	0.0048	0.0004
Ni/Al_2O_3 + Na-naphthalene-1,3, 6-trisulfonic acid	0.0076	0.0040	0.0036

with Na-saccharine refers to pure dislocation–dislocation interactions at ductile deformation. The decrease in strain-rate sensitivity with increasing strain refers to obstacles for mobile dislocations by embedded particles.

Fracture behaviour

The samples of the two composites with the high particle content (Ni/Al_2O_3 and Ni/Al_2O_3 with Na-naphthalene-1,3,6-trisulfonic acid) were strained until fracture. Figure 10 shows SEM images of the fracture interface. Both composites showed the typical jagged honey-combed structure in fracture. That indicates a ductile failure of the material, but there is no indication of a brittle fracture. Thus in both samples, a kind of compromise is accomplished between hardness and ductility.

Figure 10 shows the images of a fracture in the composites. In case of a fracture, the particles are removed from the nickel matrix without being cut. This indicates that there is no shearing mechanism for particle strengthening of the composites.

Conclusion

In this article, we have provided the proof-of-concept that Ni/Al_2O_3 composites with enhanced mechanical properties can advantageously be prepared by pulsed electro-deposition. In the case of a sufficiently high particle content in the composite, low duty cycles and rather large amounts of dispersed alumina in the plating bath are needed.

Remarkably, the addition of alumina particles and Na-saccharine to a Watts bath leads to a composite with a microstructure with grains preferentially oriented in (200)-direction perpendicular to the substrate. However, the particle content in the composite was lowered by Na-saccharine to only one-third of the value without any additive or with Na-naphthalene-1,3,6-trisulfonic acid as additive.

A particle content of about 15 vol.% increases the hardness, the wear resistance and the flow stress substantially. The probable reason for this is the high hindrance of the dislocation movement by the particles, i.e. dislocation pinning. A particle content of 5 vol.% similar to that in the composite with Na-saccharine has no effect on the wear resistance and only a marginal effect on the flow stress, but the particle content is sufficient to enhance the hardness. There is only a negligible improvement in the mechanical behaviour compared to pure nano-nickel.

As a result, for wear-resistant coatings only, the composites produced in this study with a particle content of about 15 vol.% are applicable. The composite deposited without any additive represents a kind of compromise between stiffness and fracture resistance on the one hand and wear

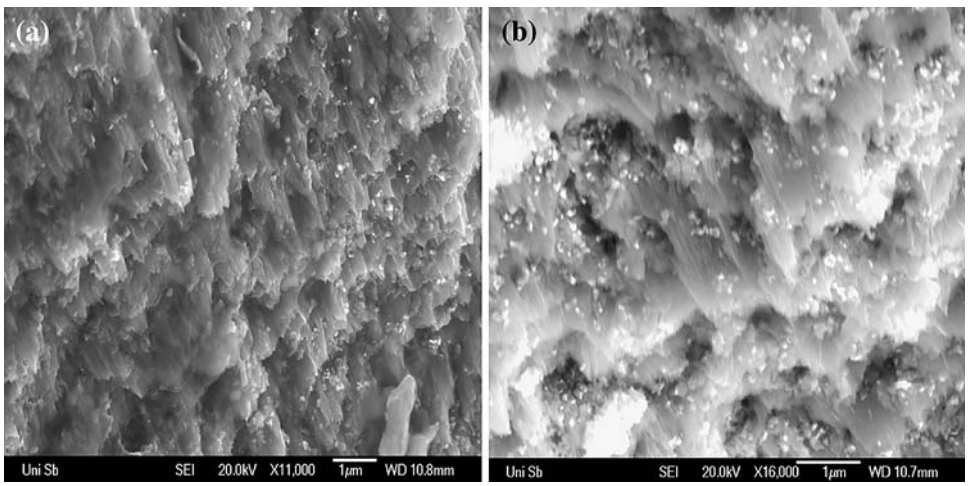

Fig. 10 SEM images of the fracture interfaces of **a** Ni/Al_2O_3 and **b** Ni/Al_2O_3 + Na-naphthalene-1,3,6-trisulfonic acid

resistance on the other hand. Due to its high hardness and, at the same time, to its ductility, it represents an interesting high performance structural material. Due to its enhanced hardness and stiffness, the composite with Na-naphthalene-1,3,6-trisulfonic acid as additive in the electrolyte is better suited for an application as a wear-resistant coating.

Acknowledgements We gratefully acknowledge the helpful discussions we had with Prof. Horst Vehoff. We thank Sylvia Kuhn for the help with electron micrographs, and Axel Bohmann for the help with the SHPB-measurements.

References

1. Sinha PK, Dhananjayan N, Chakrabarti HK (1973) Plat 60:55
2. Bahrololoom ME, Sani R (2005) Surf Coat Technol 192:154
3. Muller B, Ferkel H (2000) Mater Sci Forum 343–346:476
4. Benea L (1999) Mater Manuf Processes 14:231
5. Gay PA, Bercot P, Pagetti J (2001) Surf Coat Technol 140:147
6. Moller A, Hahn H (1999) Nanostruct Mater 12:259
7. Joshi MN, Totalani M (1979) J Electrochem Soc India 28:35
8. Babu GNKR, Muralidharan VS, Vasu KI (1991) Plat and Surf Finish 78:126
9. Medeliene V, Juskenas R, Kurtinaitiene M et al (2004) Pol J Chem 78:1305
10. Kaisheva M, Fransaer J (2004) J Electrochem Soc 151:C89
11. Ibrahim KM, Aal AA, Hamid ZA (2005) Int J Cast Met Res 18:315
12. Hu F, Chan KC (2004) Appl Surf Sci 233:163
13. Surender M, Balasubramaniam R, Basu B (2004) Surf Coat Technol 187:93
14. Stroumbouli M, Gyftou P, Pavlatou EA et al (2005) Surf Coat Technol 195:325
15. Surender M, Basu B, Balasubramaniam R (2004) Advances in surface treatment: research & applications (ASTRA). Proceedings of the international conference, Hyderabad, India, Nov 3–6, 2003, p 130
16. Endrino JL, Nainaparampil JJ, Krzanowski JE (2002) Surf Coat Technol 157:95
17. Eroglu S, Gallois B (1995) J Mater Sci 30:1754. doi:10.1007/BF00351606
18. AbiAkar H, Riley C, Maybee G (1996) Chem Mater 8:2601
19. Helle K, Walsh F (1997) Trans Inst Met Finish 75:53
20. Lee EC, Moon IT (2002) Plat Surf Finish 89:55
21. Szeptycka B, Gajewska-Midzialek A (2007) Rev Adv Mater Sci 14:135
22. Tang NK, Zhao WZ (2007) Surf Eng 23:157
23. Wang F, Arai S, Endo M (2004) Mater Trans 45:1311
24. Chen XH, Chen CS, Xiao HN et al (2005) Surf Coat Technol 191:351
25. Chen XH, Cheng FQ, Li SL et al (2002) Surf Coat Technol 155:274
26. Guo C, Zuo Y, Zhao XH et al (2007) Surf Coat Technol 201:9491
27. Chang YC, Chang YY, Lin CI (1998) Electrochim Acta 43:315
28. Chang YY, Lin CI, Chang YC (1997) J Chin Inst Chem Eng 28:245
29. Periene N, Cesuniene A, Ramanauskiene D et al (1994) Bull Electrochem 10:486
30. Szczygiel B, Kolodziej M (2005) Electrochim Acta 50:4188
31. Wang Y, Xu Z (2006) Surf Coat Technol 200:3896
32. Leo NT, Chen WP, Xiao ZY et al (2002) Trans Nonferrous Met Soc China 12:886
33. Dong SR, Tu JP, Zhang XB (2001) Mater Sci Eng A A313:83
34. Feng Y, Yuan HL, Zhang M (2005) Mater Charact 55:211
35. Schulz P (2007) Verbundwerkstoffe mit Metallmatrix. in "CCG-Seminar WB 6.06: Werkstoffe für neue Schutztechnologien". Carl-Cranz-Gesellschaft, Freiburg
36. Lach E (2007) MMC- und C/C-Werkstoffe dynamische und ballistische Eigenschaften, in "CCG-Seminar WB 6.06: Werkstoffe für neue Schutztechnologien". Carl-Cranz-Gesellschaft, Freiburg
37. Gupta S, Roy RK, Chowdhury MP et al (2004) Vac 75:111
38. Turunen E, Keskinen J, Heczko O et al (2006) Adv Eng Mater 8:669
39. Hannula SP, Turunen E, Keskinen J et al (2006) Sci Eng Ceram 317–318:539
40. Krueger HG, Knote A, Schindler U et al (2004) J Mater Sci 39:839. doi:10.1023/B:JMSC.0000012912.96350.d2
41. Sarkar P, Datta S, Nicholson PS (1997) Ceram Trans 85:231
42. Sarkar P, Datta S, Nicholson PS (1997) Composites Part B 28B:49
43. Ehrhardt J (1983) Oberfl-Surf 24:338
44. Natter H, Schmelzer M, Hempelmann R (1998) J Mater Res 13:1186
45. Natter H, Hempelmann R (2003) Electrochim Acta 49:51
46. Withers JC (1962) Prod Finish 26:62
47. Vereecken PM, Shao I, Searson PC (2000) J Electrochem Soc 147:2572
48. O'Brien DJ, Martin PW, Williams RV (1966) Appl Mater Res 5:241
49. Brandes EA, Goldthorpe D (1967) Metalurgia (Bucharest) 76:195
50. Guglielmi N (1972) J Electrochem Soc 119:1009
51. Celis JP, Roos JR, Buelens C (1987) J Electrochem Soc 134:1402
52. Hornbogen E (1985) Czech J Phys B 35:193
53. Georgiev G, Kamenova I, Georgieva V et al (2006) Godishnik na Sofiiskiya Universitet 98–99:159
54. Gladman T (1999) Mater Sci Technol 15:30
55. Orowan E (1948) Symposium on internal stresses in metals and alloys. Institute of Metals, London, p 451
56. Nembach E (1997) Particle strengthening of metals and alloys. John Wiley and Sons, New York
57. Chruschtchow MM (1957) Proc Conf Lub Wear, p 655
58. Lach E, Radjaimia A, Leitner H et al (2006) J Phys IV Proc 134:839
59. Fischer H (1954) Elektrolytische Abscheidung und Elektrokristallisation von Metallen
60. Lichtenberger A, Gazeaud G, Lach E (1988) In Dymat 88, Ajaccio